A new correction method for gamma camera non-uniformity due to energy response variability

I Buvat†, H Benali†, A Todd-Pokropek‡ and R Di Paola†

† U66 INSERM/CNRS, CHU Pitié-Salpêtrière, 91 boulevard de l'Hôpital, 75634 Paris Cédex 13, France
‡ Department of Medical Physics, University College London, Gower Street, London WC1E 6BT, UK

Abstract. We present a new uniformity correction (Fourier energy correction) which is designed to correct for gamma camera non-uniformity caused by variations of the energy response function within a wide spectral range. A convolution model is used to describe the spatial distortions of the energy response function. The model is solved in Fourier space. A preliminary flood acquisition is required to obtain energy-dependent Fourier weights which are used to correct subsequent acquisitions. The influence of the parameters involved in the correction procedure is studied and the Fourier energy correction is compared to a conventional multiplicative energy correction for different acquisition geometries. The Fourier energy correction appears especially useful when the energy information associated with each detected photon is analysed using a fine sampling, or when windows different from the photopeak window are used.

1. Introduction

Quantification in SPECT is affected by scatter, attenuation, the depth-dependent response function of the gamma camera, and reconstruction procedure. Many works are devoted to these different factors. Another important issue is the ability to obtain a spatially constant response (within the limits of Poisson statistics) over the useful detector area from a spatially constant photon flux incident on the detector. Indeed, the qualitative and quantitative performance of the imaging device depends first of all on the uniformity of its response. Three causes of non-uniformity can be distinguished:

(i) the local variations of the energy response of the camera;
(ii) the spatial distortions due to mispositioning of events; and
(iii) the variations in point sensitivity over the detector area.

It has been shown (Todd-Pokropek *et al* 1976, Wicks and Blau 1979) that the first two distortions are the most important. These are particularly of concern in SPECT, because non-uniformity distortions are magnified by the reconstruction procedure. The spatial variation of the energy response of the camera is also a problem when using scatter correction methods based on spectral analysis. Indeed, the spatial variation of the energy response results in variation of the relative positions and shapes of the local spectra across the camera face. Methods of scatter correction using spectral analysis assume that the only cause of variation in the local spectra is their relative unscatter and scatter contents. If non-uniformity also affects the local spectra, spectral analysis may be misleading (King *et al* 1992).

Several schemes of uniformity correction have been described and are implemented on commercial systems (Simmons 1988). Most scintillation cameras do not show any non-uniformity artifacts when images are acquired in the conventional photopeak window and when the energy correction is switched on. However, distortions may appear when shifting the photopeak window or when using other windows than the photopeak window (Collier *et al* 1984, Graham *et al* 1986, Hasman and Groothedde 1976, La Fontaine *et al* 1986, Sanders *et al* 1972).

This work has been motivated by the necessity of a uniform energy response within a wide spectral range as required by scatter correction methods based on spectral analysis using a fine energy sampling (Buvat *et al* 1993, Gagnon *et al* 1989, Koral *et al* 1988, Maor *et al* 1991, Wang and Koral 1992). An original methodology for correcting distortions due to non-uniformity of the energy response of the camera is described. This method is compared with the energy correction implemented on the camera both switched off and switched on. As uniformity depends on scatter, the method is evaluated for different scattering conditions. The influence of the parameters involved in the correction procedure is studied and discussed.

2. Uniformity correction

2.1. Model

Without uniformity defects, the same spectrum should be detected within every pixel of an image resulting from a 'flood' acquisition. Let $\{x_0(e)\}_{1 \leqslant e \leqslant P}$ denote this spectrum, where $x_0(e)$ is the number of events detected in energy channel e, P is the total number of energy channels, and the subscript zero characterizes non-distorted quantities. In fact, non-uniformity of the energy response of the camera leads to the detection of different spectra $\{x_i(e)\}_{1 \leqslant e \leqslant P}$ in different pixels i. A general description of energy distortion can be expressed by

$$x_i(e) = \sum_{e'} h_i(e|e')x_0(e') \tag{1}$$

where $h_i(e|e')$ is the conditional probability of detecting an event with energy e when it should have been detected with energy e' without energy distortion. If we assume that the distortion is stationary with respect to energy, i.e., that h_i does not depend on e and e' but depends only on $e - e'$, the general model (1) becomes a convolution model:

$$x_i = x_0 \otimes h_i \tag{2}$$

where $\otimes$ denotes the convolution operator.

In this convolution model, the changes in the spectra are the results of the convolution of the non-distorted spectra $\{x_0(e)\}_{1 \leqslant e \leqslant P}$ with a distortion function $\{h_i(e)\}_{1 \leqslant e \leqslant P}$, which depends on pixel i.

When imaging any source, the spectra of the photons detected in different pixels should differ from one another due to the source geometry. They should therefore depend on i and will be denoted $\{z_{0i}(e)\}_{1 \leqslant e \leqslant P}$. According to the convolution model, non-uniformity distorts these spectra so that the detected spectra $\{z_i(e)\}_{1 \leqslant e \leqslant P}$ can be written

$$z_i = z_{0i} \otimes h_i. \tag{3}$$

Using this model, the problem of non-uniformity correction can be formulated as follows: given z_i, estimate z_{0i}.

2.2. Solution

The model is solved by taking the Fourier transforms of relationships (2) and (3):

$$X_i = X_0 H_i \tag{4}$$
$$Z_i = Z_{0i} H_i \tag{5}$$

where upper-case letters represent the Fourier transforms of the corresponding lower-case quantities. H_i can be deduced from equation (4) as the ratio of X_i to X_0 and replaced in equation (5). The corrected data are then obtained by taking the inverse Fourier transform:

$$z_{0i} = \mathrm{FT}^{-1}(Z_i X_0 / X_i) \tag{6}$$

where FT^{-1} is the inverse Fourier transform operator. Consequently, the corrected data can be viewed as the original data modified by Fourier weights.

To use equation (6), the Fourier weights X_0 / X_i have to be determined from a flood acquisition. A flood acquisition using a fine energy sampling leads to the spectrum $\{x_i(e)\}_{1 \leqslant e \leqslant P}$ corresponding to each pixel i over the detector area. As these spectra are affected by Poisson noise, they are filtered using a correspondence analysis (Benali *et al* 1993) to estimate noise-free spectra $\hat{x}_i$. The reference spectrum x_0 corresponding to the spectrum that should have been detected in any pixel i is then estimated by $\hat{x}_0$, defined as the mean of the filtered spectra $\hat{x}_i$. Due to the properties of the filtering procedure (Benali *et al* 1993), the mean of the filtered spectra $\hat{x}_i$ is equal to the mean of the unfiltered spectra x_i. Indeed, the mean is supposed not to be sensitive to random noise. Finally, for each pixel i, the Fourier weight $\hat{X}_0 / \hat{X}_i$ is calculated as the ratio of the Fourier transform of the reference spectrum $\hat{x}_0$ to the Fourier transform of the filtered spectrum $\hat{x}_i$.

2.3. Implementation

The whole correction scheme works as follows:

Fourier weights acquisition.

(i) A flood acquisition is performed using a fine spectral sampling, leading to a set of spectra $\{x_i(e)\}_{1 \leqslant e \leqslant P}$ corresponding to each pixel i over the detector area.

(ii) These spectra are filtered using a correspondence analysis (Benali *et al* 1993) to estimate noise-free spectra $\hat{x}_i$.

(iii) A reference spectrum x_0 is estimated by $\hat{x}_0$, defined as the mean of the filtered spectra $\hat{x}_i$ (or the mean of the non-filtered spectra).

(iv) The values of $\hat{X}_0 / \hat{X}_i$ are calculated and stored as the Fourier weights.

Correction procedure.

(i) For each pixel i, the Fourier transform Z_i of the spectrum z_i of the photons detected in this pixel is calculated using the same energy sampling as that used for the Fourier weight computation.

(ii) Z_i is multiplied by the Fourier weight associated with pixel i and the inverse Fourier transform of $Z_i \cdot \hat{X}_0 / \hat{X}_i$ is computed to obtain the corrected spectrum $\hat{z}_{0i}$ for pixel i.

After this correction procedure, the energy of the detected events is available for any pixel with a sampling equal to the sampling used for the correction. It can be analysed for energy discrimination or spectral analysis. This correction procedure will subsequently be referred to as the Fourier energy correction (FEC).

3. Assessment of the method

3.1. Computation of the Fourier weights

A ^{99}Tc^m flood acquisition was performed using a point source located in front of a DSX Sopha camera without any collimator. 30 million events were acquired in the 40–236 keV range, using list mode recording position, energy and time for each detected photon. For this acquisition, denoted Foff, the energy correction implemented on the camera was switched off. The Fourier weights corresponding to a 4 keV sampling, in the 44–160 keV spectral range, were derived as explained previously. 73 312 values (2528 pixels in the field of view and 29 energy channels) were stored for correcting subsequent acquisitions.

3.2. Uniformity assessment for flood acquisition

The flood acquisition was repeated with the energy correction implemented on the camera switched on. This acquisition is denoted Fon. The energy correction built into the camera was a multiplicative correction, which will be presented in more detail in the discussion. The uniformity of the spectral response of the camera measured using a flood source was compared in three instances:

   (i) flood acquisition with energy correction switched off (Foff);
   (ii) flood acquisition with energy correction switched on (Fon); and
   (iii) flood acquisition with energy correction switched off postprocessed by FEC.

Uniformity of flood images was quantified by a uniformity index v defined by:

$$v = \sigma/\bar{n}^{1/2} \tag{7}$$

where $\bar{n}$ is the mean number of counts per pixel and σ is the standard deviation of the number of counts per pixel in the field of view of the camera. For a flood image that is only affected by statistical fluctuations (Poisson statistics), the theoretical value of v is unity.

   As uniformity depends on energy window, v was calculated for each 4 keV window from 44 to 160 keV and was represented as a function of energy.

3.3. Uniformity assessment for Phelps phantom acquisition

To assess the reliability of uniformity correction for different imaging geometries, a Phelps phantom was imaged. The phantom consisted of seven cold plastic rods with diameters equal to 5, 7.5, 10, 15, 20, 25 and 30 mm, which were embedded in a cylindrical Perspex container containing a ^{99}Tc^m background. Two list mode acquisitions including two million events were performed in a wide energy window of 40–236 keV. For the first acquisition (Poff), the energy correction was switched off, whereas it was switched on for the second (Pon). A region of interest (ROI) of 419 pixels was drawn over the background of the phantom. The uniformity index v was calculated for the pixels within this background ROI. The uniformity index was measured and represented as a function of energy between 44 and 160 keV in three instances:

   (i) Phelps phantom acquisition with energy correction switched off (Poff);
   (ii) Phelps phantom acquisition with energy correction switched on (Pon); and
   (iii) Phelps phantom acquisition with energy correction switched off postprocessed by FEC.

For these three cases, three images were also created:

(i) the image corresponding to a photopeak window (124–156 keV) (this energy range corresponds to a ∼ 23% wide spectral window centred on 140 keV);

(ii) the image corresponding to the lower half of the photopeak window (124–140 keV); and

(iii) the image corresponding to the upper half of the photopeak window (140–156 keV).

The histograms of the number of events within the background ROI were represented for the nine resulting images. As the background ROI is assumed to contain uniform activity, these histograms should display Gaussian shapes.

3.4. Parameters affecting the correction

Several aspects of the Fourier energy correction were investigated, namely the influence of the filtering step used before calculating the Fourier weights, the comparison of correction applied to data acquired with and without the energy correction switched on, the reliability of the correction with respect to the amount of scattering and to the counting statistics, the spectral sampling, and the consequences of the Fourier energy correction on the energy resolution.

3.4.1. The influence of the filtering step. In the method as has been presented, the Fourier weights are calculated from the spectra filtered by a correspondence analysis. To demonstrate the importance of the filtering step, we computed the Fourier weights X_0/X_i from the same flood acquisition, but without filtering the spectra. The absence of filtering does not affect the reference spectrum x_0, since the mean of the filtered spectra $\hat{x}_i$ is equal to the mean of the unfiltered spectra x_i. However, on the denominator of the Fourier weights, $\hat{X}_i$ is different from X_i. The Phelps phantom acquisition Poff was corrected using these non-filtered Fourier weights. The results were compared with those obtained from the same acquisition corrected using the filtered Fourier weights. In both cases, the uniformity index was plotted against energy with a 4 keV sampling.

3.4.2. Correction of the precorrected data. Fourier energy correction of data acquired with the energy correction switched off was compared with FEC applied to data previously corrected by switching on the built-in energy correction. For this investigation, Fourier weights were derived from the flood acquisition with energy correction on (Fon). Uniformity was measured in four configurations: Foff, Fon, Foff corrected with Fourier weights derived from Foff acquisition, and Fon corrected with Fourier weights derived from Fon acquisition. We also compared uniformity for the Phelps acquisition Pon corrected with Fourier weights derived from Fon with that for the Phelps acquisition Poff corrected with Fourier weights derived from Foff.

3.4.3. The amount of scattered radiation. The Fourier weights are calculated from a flood acquisition and are assumed to be appropriate for correction of any subsequent acquisitions, regardless of the acquisition geometry. The validity of this assumption was studied by comparing the results of FEC for different acquisition geometries. The flood acquisition Foff used to compute the Fourier weights corresponds to a specific geometry G1. The Phelps phantom acquisition Poff corresponds to another geometry G2. A third acquisition, corresponding to a geometry G3, was performed. The same Phelps phantom was used,

but a scatter medium (Perspex slab) was added between the top of the phantom and the collimator of the camera. Data were acquired with energy correction switched off, and corrected subsequently using the Fourier weights derived from Foff. The different scattering amounts were qualitatively estimated by looking at the total spectra for the three geometries G1, G2, and G3. The uniformity indices for the Phelps phantom acquisitions corresponding to geometries G2 and G3 and corrected by the Fourier weights derived from geometry G1 were compared.

3.4.4.   Counting statistics.   The number of events that should be acquired during the flood acquisition used to calculate the Fourier weights is an important issue. Indeed, the Fourier weights should be robust enough to ensure a proper correction of subsequent acquisitions, whatever the counting statistics. Using the Fourier weights calculated from the 30 million counts flood acquisition Foff, we corrected Phelps acquisitions (Poff, G2 geometry) including 100 000, 500 000, two million and 30 million events in the 40–236 keV spectral range. We compared the uniformity indices plotted against energy before and after FEC. We also represented ν as a function of the ratio R of the mean number of events per pixel in the background of those Phelps acquisitions which had to be corrected, $\bar{z}_{bgd}(e)$, to the mean number of events per pixel when calculating the Fourier weights, $\bar{x}(e)$. These mean values were calculated for each 4 keV image.

3.4.5.   Energy sampling.   Two experiments were conducted for studying the energy sampling to be used for calculating the Fourier weights and performing FEC. The 80–160 keV range was considered. In a first experiment, Fourier weights were calculated from acquisition Foff with an 8 keV and a 4 keV sampling respectively. Corrections of Foff, Poff-G2, and Poff-G3 were performed using these two samplings. Uniformity was then quantified for 8 keV wide images resulting from the corrections.

The second experiment followed the same principle but evaluated uniformity for a 4 keV sampling. Fourier weights were calculated from Foff with a 4 keV and a 2 keV sampling respectively. Data were corrected using these two samplings before quantifying uniformity in 4 keV wide images.

3.4.6. Energy resolution.   As the reference spectrum used to derive the Fourier weights is calculated from the mean of the individual local spectra, it is expected that this reference spectrum will have a larger full width at half maximum (FWHM) than the individual spectra if some of those individual spectra are shifted in energy. Therefore, the Fourier energy correction may affect the energy resolution of the camera. This effect was quantified by calculating the mean FWHM and the associated standard deviation over the 2528 individual spectra in the field of view for Foff, Fon, and Foff after FEC. The FWHM values were expressed as energy resolution at 140 keV using

$$\text{energy resolution} = 100 \text{ FWHM}/140. \tag{8}$$

4. Results

4.1. Flood acquisition

Figure 1 shows the values of the uniformity index for each 4 keV image from 44 to 160 keV for the flood source acquired without energy correction (Foff), with energy correction (Fon), and without energy correction followed by FEC. Uniformity is strongly dependent on energy
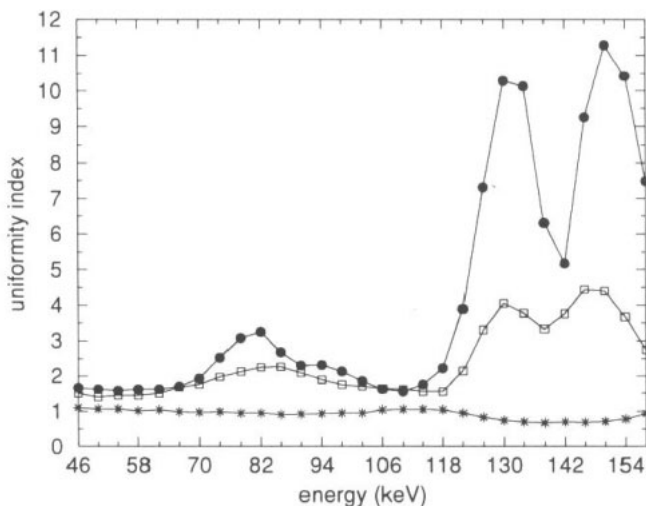
Figure 1. Uniformity index as a function of energy for flood source acquisitions: ●, without energy correction (Foff); □, with multiplicative energy correction (Fon); *, without energy correction and postprocessed by FEC.

when FEC is not performed. After FEC, the response of the camera is uniform (ν close to unity) whatever the energy range. The images corresponding to the 128–132 keV spectral range are presented in figure 2, as a typical example of the quality of the different images.
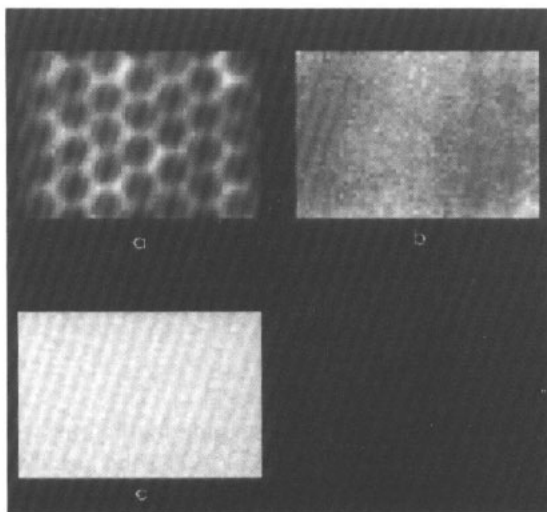
Figure 2. Flood source images corresponding to the 128–132 keV spectral range: (a) without energy correction (Foff); (b) with multiplicative energy correction (Fon); (c) without energy correction and postprocessed by FEC.
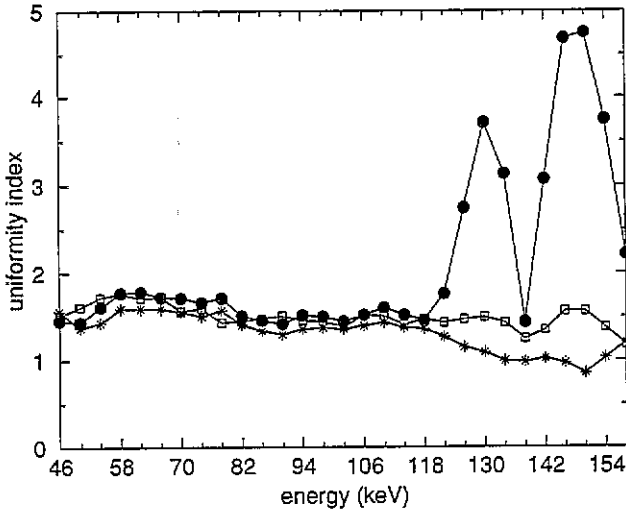
Figure 3. Uniformity index as a function of energy for Phelps phantom acquisitions: ●, without energy correction (Poff); □, with multiplicative energy correction (Pon); *, without energy correction and postprocessed by Fourier energy correction (Poff+FEC).

4.2. Phelps phantom acquisition

The uniformity index v for the background ROI of the Phelps phantom image is plotted against energy for the acquisition with energy correction switched off (Poff), switched on (Pon), and switched off followed by FEC (figure 3). FEC results in an improvement of the uniformity of the camera response, especially in the 116–160 keV spectral range. When considering the photopeak image, no great difference in the distribution of counts in the background ROI is observed (figure 4). The photopeak images look also very similar without and with energy correction (figure 5). On the other hand, the distribution of background counts departs significantly from a Gaussian distribution in the two half photopeak images when no correction is applied (figure 4) and uniformity artifacts are striking on the images (figure 5). When the energy correction is switched on (Pon), the departure from a Gaussian distribution is much less marked. The images do not present the photomultiplier tube pattern but slowly varying uniformity defects can be seen. FEC sharpens the distribution of background counts towards a Gaussian shape, and the corresponding images do not present any uniformity artifact.

4.3. Parameters affecting the correction

4.3.1. The influence of the filtering step. When computing the Fourier weights from non-filtered data, some $X_i(v)$ values turned out to be zero. When this occurred, $X_0(v)/X_i(v)$ was replaced by unity, so that the corresponding value $Z_i(v)$ remained unchanged during the correction. When correcting Poff acquisition, outlier values appeared in the corrected 4 keV images, namely pixels with values equal to zero or greater than 1000 in the background ROI where the mean values varied from ~ 30 at 44–48 keV to ~ 350 at 136–140 keV. These outlier values were replaced by their original values in order not to severely affect the index v. After these substitutions, v was calculated and plotted against energy (figure 6). We also plotted the minimum, mean, and maximum values for the pixels within the background
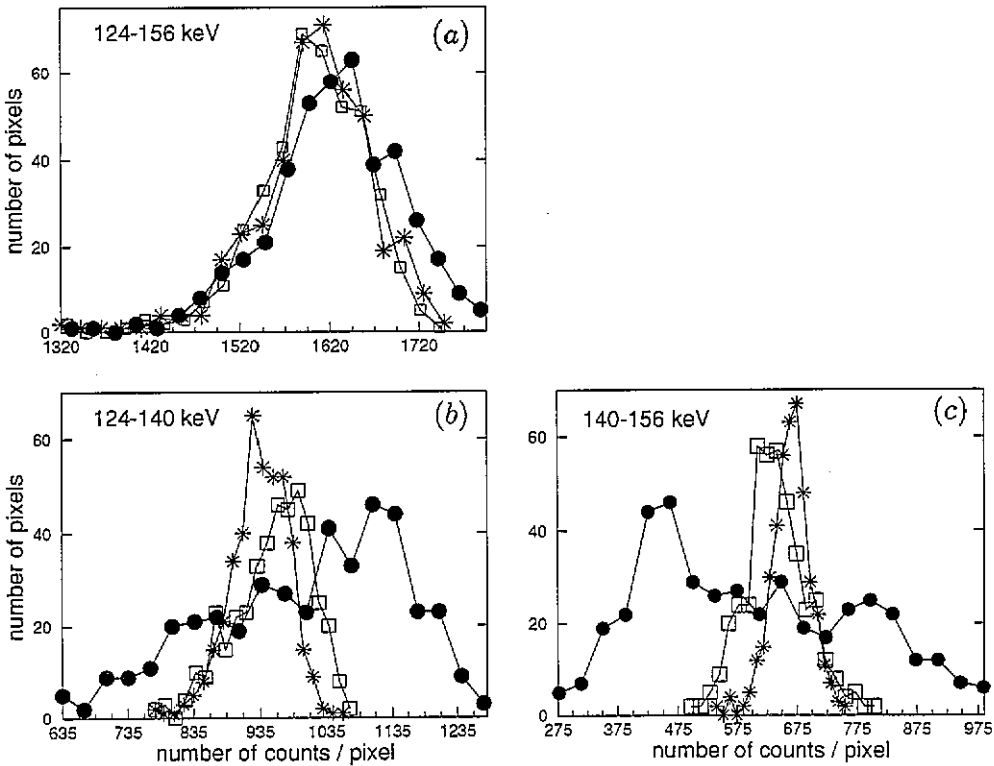
Figure 4. Hisotgrams of the number of counts per pixel in the background ROI of the Phelps phantom for (a) the photopeak image, (b) the lower-half-photopeak image, and (c) the upper-half-photopeak image: ●, without energy correction (Foff); □, with multiplicative energy correction (Fon); *, without energy correction and postprocessed by FEC.

ROI against energy (figure 7). When using the non-filtered Fourier weights, these values were computed after removing the outlier values. The serrated shape of the minimum and maximum values observed when no filtering was performed shows that the non-filtered Fourier weights include outlier values that would introduce artifacts in the corrected images.

4.3.2. Correction of the precorrected images. A comparison of uniformity depending on whether FEC is applied to raw (Foff, Poff) or precorrected data (Fon, Pon) is shown in figure 8. In the instance of the flood source, FEC of raw data performs consistently better than correction of precorrected data (figure 8(a)). The same tendency is observed for the Phelps phantom (figure 8(b)), although it is less marked.

4.3.3. The amount of scattered radiation. The different scattering conditions corresponding to acquisition geometries G1, G2, and G3 are illustrated in figure 9. The spectra are those of all detected photons for each experiment (Foff, Poff-G2, Poff-G3). There are normalized to better display the different scatter proportions.

Results of FEC for both G2 and G3 geometries are shown in figure 10. FEC improves uniformity for any energy range, except for 44–48 keV and 156–160 keV images. The background ROI is more uniform in G3 geometry, i.e., when the scatter proportion is the greatest.
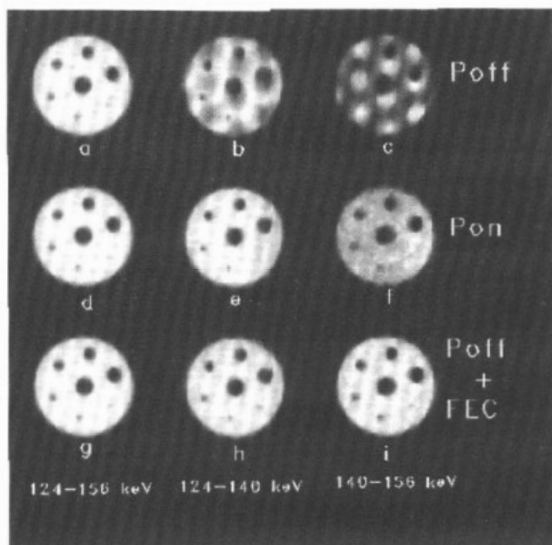
Figure 5. Photopeak, lower-half-photopeak, and upper-half-photopeak images of the Phelps phantom: (a)–(c) without energy correction (Poff); (d)–(f) with multiplicative energy correction (Pon); (g)–(i) without energy correction and postprocessed by Fourier energy correction (Poff+FEC).
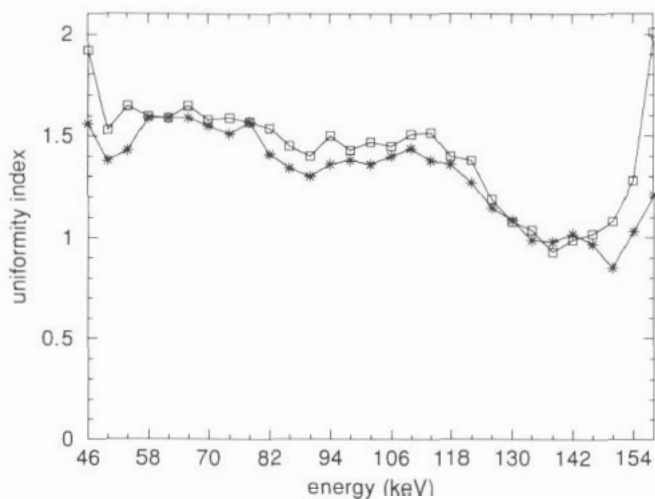
Figure 6. Uniformity index as a function of energy for the Phelps phantom acquisition corrected with Fourrier weights: □, computed from non-filtered data; *, computed from filtered data.

4.3.4. Counting statistics. Uniformity index before and after FEC is plotted against energy for Poff acquisitions corresponding to four different counting statistics (figure 11). With or without FEC, the greater the counting statistics, the more marked the uniformity defects. After FEC, uniformity index is close to unity for the 100 000, 500 000, and two million count acquisitions. For the 30 million count acquisition, uniformity defects remain unacceptable ($v > 2$) after FEC, although they have significantly decreased with respect to those observed
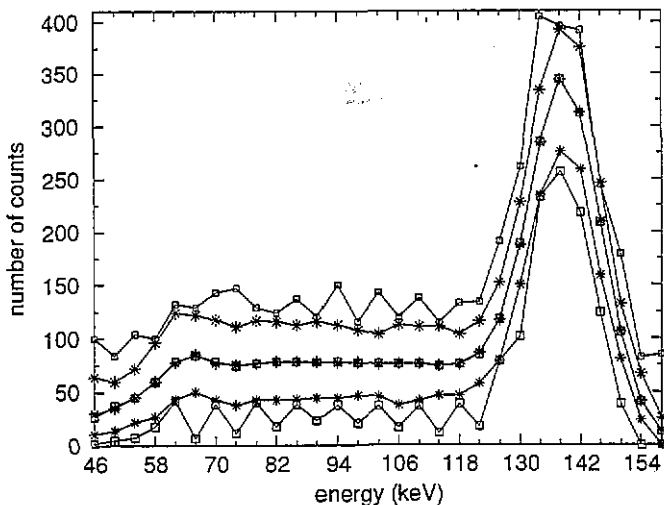
Figure 7. Minimum, mean, and maximum values in the pixels belonging to the background ROI of Phelps phantom images for data corrected with Fourier weights: □, computed from non-filtered data; * computed from filtered data.
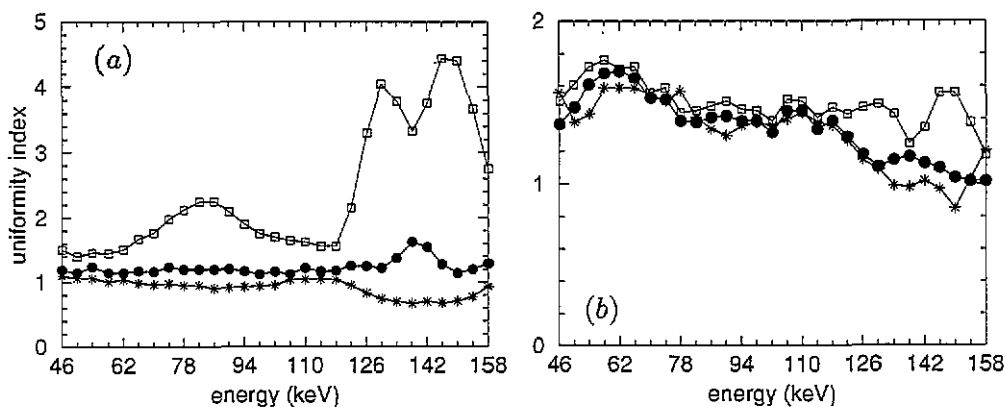
Figure 8. Uniformity index as a function of energy for three correction procedures: □, multiplicative energy correction; ●, multiplicative energy correction followed by FEC; *, FEC. (a) Flood acquisition; (b) Phelps phantom acquisition.

before correction.

When plotting υ after FEC against the ratio $R = \bar{z}_{\mathrm{bgd}}(e)/\bar{x}(e)$, a relationship between these two quantities clearly appears (figure 12). This plot especially shows that uniformity defects are not properly corrected when $\ln R > 0$, i.e., when $R > 1$.

4.3.5. Energy sampling. A comparison of uniformity after FEC in 8 keV wide and 4 keV wide images is shown in figure 13, for different sampling procedures. In 8 keV wide images, calculating the Fourier weights with a 4 keV sampling leads to more uniform images than when the Fourier weights are calculated with a 8 keV sampling: oversampling from 8 keV to 4 keV is beneficial. When one considers uniformity in 4 keV wide images, there is no need
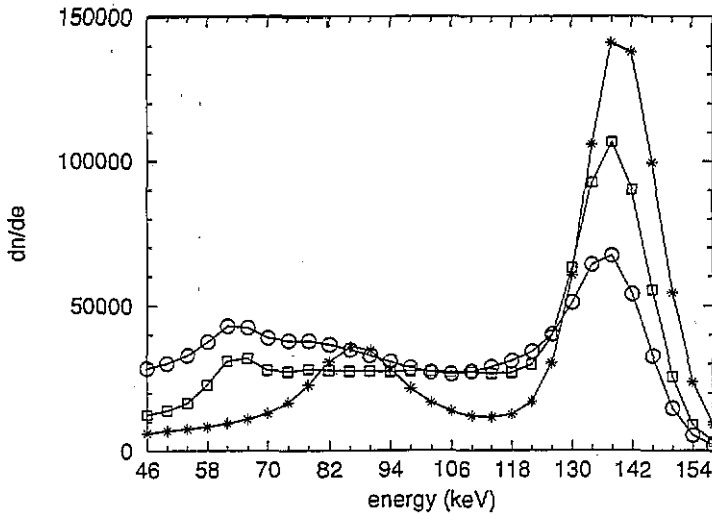
Figure 9. Spectra of all detected photons for three acquisitions geometries: ∗, flood acquisition G1 (low scatter proportion); □, Phelps phantom G2 (medium scatter proportion), O, Phelps phantom G3 (high scatter proportion). The three spectra are normalized so that their integrals are the same.
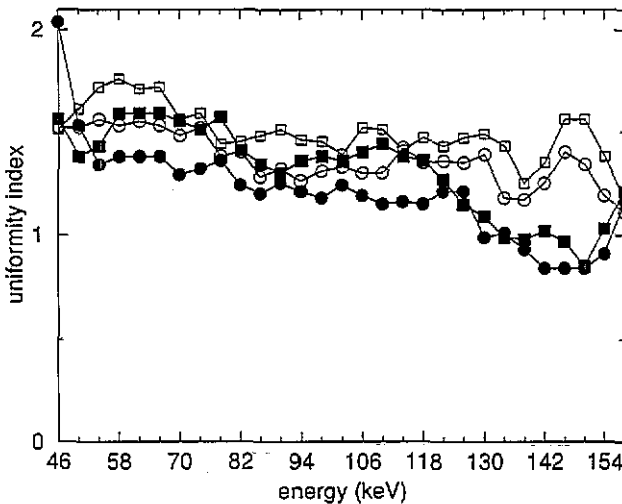
Figure 10. Uniformity index as a function of energy for Phelps phantom acquisitions corresponding to geometries G2 (without additional scatter medium) and G3 (with additional scatter medium) with multiplicative energy correction (□, Pon G2; O, Pon G3) and with FEC (■, Poff G2+FEC; ●, Poff G3+FEC).

to use 2 keV sampling when computing the Fourier weights: no significant improvement results from over-sampling from 4 keV to 2 keV.

4.3.6. Energy resolution. Before correction (Foff), the mean energy resolution over the field of view of the camera is 11.8% at 140 keV, with a standard deviation equal to 0.8%.
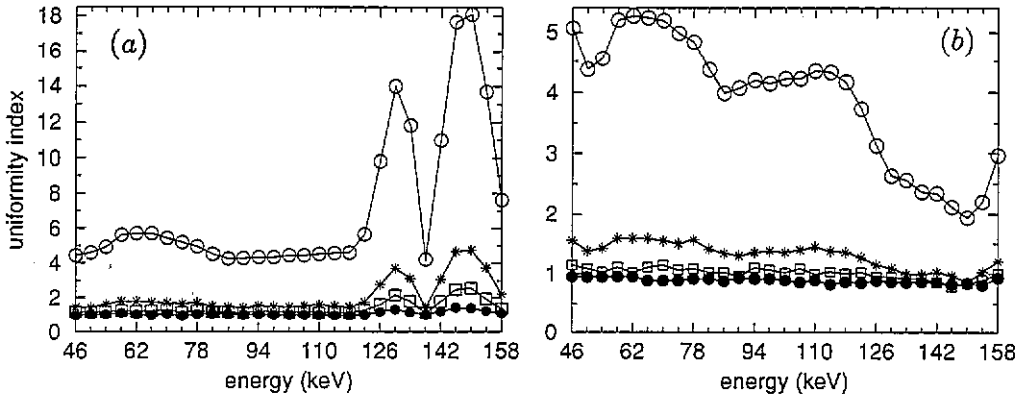
Figure 11. Uniformity index as a function of energy and for different counting statistics (*a*) before FEC and (*b*) after FEC. Acquisitions include 100 000 counts (●), 500 000 counts (□), two million counts (∗) and 30 million counts (O).

With energy correction switched on (Pon), the mean energy resolution is 12.8% and the associated standard deviation is 1.2%. After FEC (Poff followed by FEC), the mean energy resolution is 12.6% with a 0.4% standard deviation.
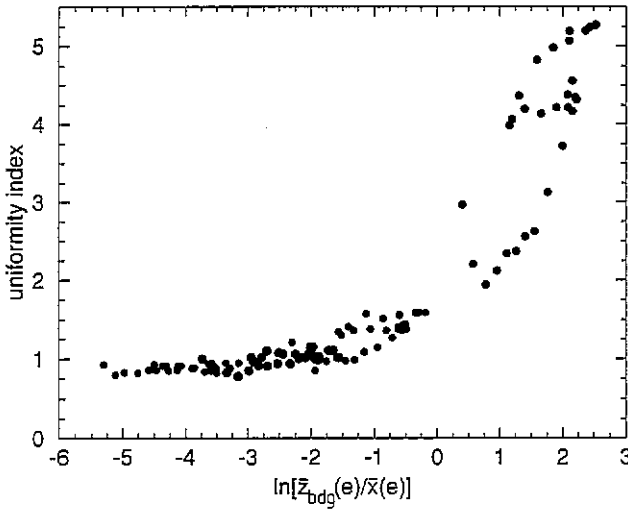
Figure 12. Uniformity index plotted against the ratio $R = \bar{z}_{bgd}(e)/\bar{x}(e)$. $\bar{z}_{bgd}(e)$ is the mean number of events per pixel in the background of those Phelps acquisitions which have to be corrected, and $\bar{x}(e)$ is the mean number of events per pixel when calculating the Fourier weights.

5. Discussion

Uniformity of the response of a gamma camera is strongly dependent on the spectral range in which this response is observed (Collier *et al* 1984, Graham *et al* 1986, Hasman and Groothedde 1976, La Fontaine *et al* 1986, Sanders *et al* 1972). This results from the fact
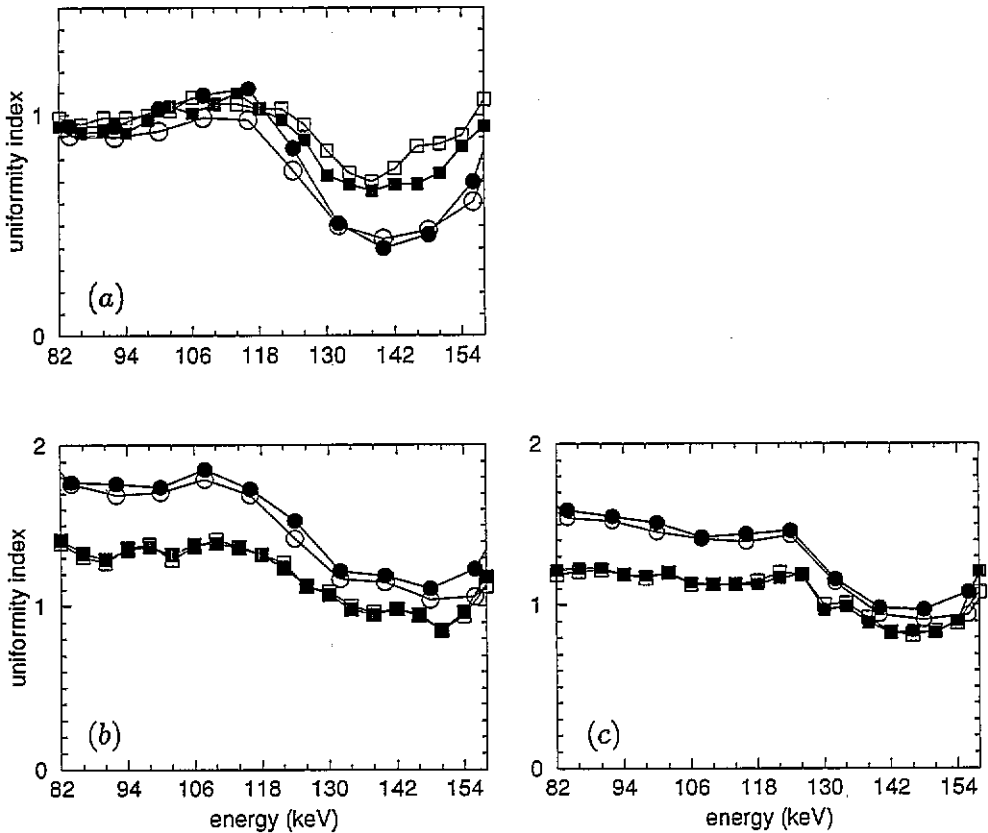
Figure 13. The influence of energy sampling used for FEC: uniformity index measured on 8 keV wide images after correction with 8 keV sampled Fourier weights (●) and 4 keV sampled Fourier weights (○); uniformity index measured on 4 keV wide images after correction with 4 keV sampled Fourier weights (■) and 2 keV sampled Fourier weights (□). (*a*) Flood acquisition; (*b*) Phelps phantom G2 acquisition; (*c*) Phelps phantom G3 acquisition.

that a major cause of non-uniformity is the variation in the positions and shapes of the spectra recorded at different spatial locations over the detector area. This effect can be compensated for by adjusting the position (Todd-Pokropek *et al* 1976) or the position and the width of the acquisition energy window as a function of the pixel (Knoll *et al* 1979). In these approaches, the spectra corresponding to each pixel of a matrix covering the detector area are recorded. The position and width of the photopeak are determined for each pixel spectrum. Correction factors giving the shift and the width of the energy window for each pixel are deduced and stored in a look-up table. During subsequent acquisitions, the look-up table is consulted for each detected event, to establish whether the event falls into the spectral window. In this sliding window method, events detected with the same energy signal may be included in one pixel and not in another. Another procedure addressing the issue of energy response variability modifies the energy information associated with detected events. The energy e associated with each event is replaced by $e + \Delta_i$, where Δ_i depends on the pixel i. Δ_i may also depend on the energy e: in this case (called multiplicative correction), Δ_i is expressed as $k_i e$, where the factor k_i is determined for each pixel i. When Δ_i does not depend on e, this correction scheme is equivalent to that of the constant-width

sliding window, with an energy shift equal to Δ_i for pixel i.

The constant-width sliding window correction assumes that energy non-uniformity can be fully described by energy shifts of the detected spectra. It does not account for the shape variability (resulting for instance from spatial variations of the energy resolution). When the width of the window is also modified from one pixel to another, the spatial variations of energy resolution of the camera can be taken into account. In the multiplicative correction procedure, which replaces e by $e + k_i e$, the energy distortion is assumed to be proportional to the detected energy, and the energy information e is then changed for $(1 + k_i)e$. The distortions modelled by the sliding window with variable width and by the multiplicative correction correspond to a shift dilation or a shift contraction of the spectra. The model we propose is more comprehensive in that it accounts for distortions that cannot be described by a single multiplicative coefficient. While the sliding window and the multiplicative corrections only require one or two parameters per pixel to be determined (window shift, window width, or k_i), the Fourier energy correction relies on P Fourier weights per pixel, where P represents the number of energy channels which are considered. In practice, $2P$ parameters must be stored because each Fourier weight consists of a real and an imaginary part. Alternatively, only P values can be used by taking advantage of the symmetry properties of the Fourier transform of real signals.

A full description of energy distortion would necessitate the model given by equation (1). This solution of this model requires the determination and storage of a $P \times P$ matrix per pixel $h_i(e|e')$ and could be approached as an inverse problem.

The convolution model is a particular case of the general model (1). It assumes that the energy distortion is stationary with respect to energy, as opposed to the non-stationary model described by equation (1). The energy shift of the spectra, as handled by the constant-width sliding window correction is a particular case of the convolution model. It corresponds to $h_i(e) = \delta(e + \Delta_i)$, where Δ_i represents the energy shift and δ is the Dirac delta function.

The relevance of the convolution model was studied in comparison with the multiplicative correction implemented on the camera which was used for conducting the experiments. The flood acquisition demonstrates that non-uniformity is severely dependent on energy without correction and also with multiplicative correction (figure 1). The greater the scatter proportion, the less marked this dependence, as observed when comparing the values of u for the flood, G2, and G3 Phelps acquisitions (figure 10). However, these results confirm the need for an appropriate energy correction when one is interested in analysing local fine-sampled spectra and/or data recorded in narrow or non-conventional (i.e., different from the photopeak) energy windows. Despite underlying non-uniformity, images corresponding to wider spectral windows (especially to the photopeak window) may not display marked uniformity artifacts (figures 4 and 5). Indeed, the artifacts observed for narrow energy windows may cancel out when adding the events recorded in these spectral windows.

The assessment of FEC shows that it performs as well as multiplicative correction or better than it over a wide spectral range. The uniformity improvement resulting from FEC is especially noticeable between 112 and 156 keV. Therefore, FEC turns out to be of value not only when processing data belonging to a wide spectral range, but also when handling energy information in the photopeak spectral range. The smaller improvement that has been observed with the Phelps acquisition below 112 keV may be explained as follows: it was assumed that the background ROI used to calculate υ should contain a spatially uniform signal. Though the $^{99}Tc^m$ activity was uniformly distributed in the background of the Phelps phantom, this does not ensure that signal detected in front of the background area is also uniform because of scatter and edge effects. Consequently, in the spectral

range corresponding to scattered photons, the background ROI may contain signal which is intrinsically non-uniform, and the values v as calculated may not be theoretically equal to unity.

Several features of the FEC have been investigated. The filtering step is necessary for the Fourier weights to be robust (figure 6). A correspondence analysis was used for estimating the noise-free component of the spectra recorded with the flood acquisition. Indeed, this has been demonstrated to be the optimal orthogonal decomposition for scintigraphic data given their statistical properties (Benali *et al* 1993). However, other filtering procedures to estimate the noise-free spectra could be studied.

As the convolution model does not exactly model the shift dilation or the shift contraction handled by multiplicative correction, we compared FEC applied to raw data with FEC applied to data resulting from the multiplicative correction. There is no advantage in performing both corrections. FEC alone performs better when applied to raw data. The multiplicative correction may transform the spectra so that the convolution model is no longer appropriate.

The proportion of scatter when acquiring the flood source is low (figure 9). It was necessary to study whether the Fourier weights derived from this 'low-scatter' geometry could properly process acquisitions for which a greater amount of scatter is detected. FEC is effective for very different scatter proportions (figures 9 and 10). In any case (without correction, with multiplicative or FE correction), non-uniformity is less pronounced when the amount of scatter increases. This may result from the fact that scatter makes the uniformity defects less visible by blurring the images.

The Fourier weights should be calculated from a flood acquisition containing as many events as possible. The more events, the more apparent the uniformity defects. The Fourier weights are then more able to precisely describe the distortions, and will be more robust for processing subsequent acquisitions. From figure 12, it can be seen that a robust correction requires that, for each energy channel, the number of photons in a pixel of the acquisition to be processed should always be less than the mean number of photons per pixel used for calculating the Fourier weights. The proportion of scatter/photopeak events is lower in flood acquisition than in clinical acquisitions. Consequently, this is the mean number of events per pixel in the Compton spectral range which has to be greater for the flood acquisition than for patients acquisitions and which should determine the number of events to be acquired for the Fourier weights computation. If this requirement is met, a robust correction will also be ensured in the photopeak spectral range, since the proportion of photopeak/scatter events is greater for the flood acquisition than for patients' acquisitions.

Regarding the spectral sampling to be used for the calculation of the Fourier weights and for correcting the data, 4 keV appeared to be a proper choice. 2 keV sampling does not significantly improve the uniformity of corrected images, whereas a coarser sampling (e.g., 8 keV) degrades it.

The improvement in spatial uniformity for any energy range obtained with FEC results from the recovery of a uniform energy response function over the field of view of the camera. This spatially uniform energy response function is estimated from a reference spectrum which is the mean of the individual local spectra. Therefore, the FWHM of the reference spectrum will be larger than the FWHM of the individual spectra if some of those individual spectra are shifted in energy. As the FWHM measures the energy resolution of the camera, the energy resolution is expected to be poorer after FEC than before. Measurements confirmed this expectation (the mean energy resolution at 140 keV is equal to 12.6% after FEC against 11.8% before). The degradation of the mean energy resolution resulting from FEC is comparable to that observed when using the multiplicative energy

correction (12.8%). Before energy correction, the standard deviation of the energy resolution over the field of view is low (0.8%), which means that most of the uniformity defects are caused by energy shifts of the individual spectra rather than by changes in the FWHMs of those individual spectra. The improvement in uniformity obtained with the multiplicative correction results from the correction for these energy shifts, but this correction goes along with greater variations of the FWHM of the individual spectra, as reflected by the increase of the standard deviation of the energy resolution (1.2%). In other words, in the multiplicative correction, the energy shifts are corrected for mainly by locally widening the photopeak, which makes the FWHM more variable. FEC corrects for energy non-uniformity by reducing both the energy shifts and the local variations of the FWHM (standard deviation of the energy resolution equal to 0.4%).

The FEC scheme as described in this work could be implemented as an automatic postprocessing procedure. Since the Fourier transform of the individual local spectra is required to apply the Fourier weights and complete the correction, an on-line correction is not possible. However, as the Fourier transform is a fast operation, it is conceivable to perform the energy correction several times during the acquisition, based on the previously stored spectral data, to provide the user with intermediate corrected images. The energy sampling required by the procedure (typically 4 keV sampling) could be implemented either as a list mode acquisition or as a multiwindow acquisition. While the former approach offers more possibilities for research purpose, the latter solution is more efficient for routine use. Indeed, sampling can be performed when digitizing the energy information, and does not require sorting of the data at the end of the acquisition. It also saves storage space since the same space is required to store and process the spectra regardless of the acquired number of counts.

6. Conclusion

A new procedure for the correction of camera non-uniformity resulting from local variations of the energy response has been described. It relies on the assumption that the distortions of each local spectrum can be modelled by the convolution of the non-distorted spectrum with a distortion function depending on the pixel. The model is solved in Fourier space using data obtained from a flood acquisition. Those data must be appropriately filtered to obtain robust energy dependent Fourier weights. The influence of the parameters involved in the correction procedure have been investigated. The Fourier energy correction appears to be especially of value when the energy information associated with each detected photon is analysed using a fine sampling, or when windows different from the photopeak window are used. Indeed, FEC considerably reduces the dependence of uniformity on spectral range and results in a uniform response of the camera over a wide spectral range and for any spectral window.

In the work presented here, the Fourier weights have been calculated for ^{99}Tc^m acquisitions in a 44–160 keV range and used to correct ^{99}Tc^m acquisitions. Further experiments should determine whether the Fourier weights can also successfully correct acquisitions performed in the same spectral range but using other radioisotopes (e.g., ^{123}I, ^{201}Tl).

The Fourier energy correction does not address non-uniformity resulting from mispositioning events (i.e., linearity defects). It is only an energy correction that should be used along with a correction for geometric distortions.

Acknowledgments

References

Benali H, Buvat I, Frouin F, Bazin J P and Di Paola R 1993 A statistical model for the determination of the optimal metric in factor analysis of medical image sequences (FAMIS) *Phys. Med. Biol.* **38** 1065–80
Buvat I, Benali H, Frouin F, Bazin J P and Di Paola R 1993 Target apex-seeking in factor analysis of medical image sequences *Phys. Med. Biol.* **38** 123–38
Collier B D, Palmer D W, Knobel J, Isitman A T, Hellman R S and Zielonka J S 1984 Gamma camera energy for Tc^{99m} bone scintigraphy: effect of asymmetry on contrast resolution *Radiology* **151** 495–7
Gagnon D, Todd-Pokropek A, Arsenault A and Dupras G 1989 Introduction to holospectral imaging in nuclear medicine for scatter subtraction *IEEE Trans. Med. Imaging* **MI-8** 245–50
Graham L S, La Fontaine R L and Stein M A 1986 Effects of asymmetric photopeak windows on flood field uniformity and spatial resolution of scintillation cameras *J. Nucl. Med.* **27** 706–13
Hasman A and Groothedde R T 1976 Gamma-camera uniformity as a function of energy and count-rate *Br. J. Radiol.* **49** 718–22
King M A, Hademenos G J and Glick S J 1992 A dual-photopeak window method for scatter correction *J. Nucl. Med.* **33** 605–12
Knoll G F, Bennett M C, Koral K F and Strange D R 1979 Removal of gamma camera nonlinearity and nonuniformities through real-time signal processing *Information Processing in Medical Imaging* ed R Di Paola and E Kahn (Paris: INSERM) pp 187–200
Koral K F, Wang X, Rogers W L, Clinthorne N H and Wang X 1988 SPECT Compton- scattering correction by analysis of energy spectra *J. Nucl. Med.* **29** 195–202
La Fontaine R, Stein M A, Graham L S and Winter J 1986 Cold lesions: enhanced contrast using asymmetric photopeak windows *Radiology* **160** 255–60
Maor D, Berlad G, Chrem Y, Voil A and Todd-Pokropek A 1991 Klein–Nishina based energy factors for Compton free imaging (CFI) *J. Nucl. Med.* **32** 1000 (Abstract)
Sanders T P, Sanders T D and Kuhl D E 1972 Optimizing the window of an Anger camera for ^{99m}Tc *J. Nucl. Med.* **12** 703–6
Simmons G H 1988 On-line corrections for factors that affect uniformity and linearity *The Scintillation Camera* ed G H Simmons (New York: Society of Nuclear Medicine) pp 46–59
Todd-Pokropek A E, Erbsmann F and Soussaline F 1976 The non-uniformity of imaging devices and its impact in quantitative studies *Medical Radionuclide Imaging* (Vienna: IAEA) pp 67–82
Wang X and Koral K F 1992 A regularized deconvolution-fitting method for Compton- scatter correction in SPECT *IEEE Trans. Med. Imaging* **MI-11** 351–60
Wicks R and Blau M 1979 Effect of spatial distortion on Anger camera field uniformity correction: concise communication *J. Nucl. Med.* **20** 252–4